Page 1 of 31. © Royal Aeronautical Society YYYY
doi: 10.1017/aer.2016.1

Characterization of the Eddy Dissipation Model for the Design of Hydrogen-fueled Scramjets

J.J.O.E Hoste[*], **M. Fossati**

University of Strathclyde
Department of Mechanical and Aerospace Engineering, Aerospace Centre of Excellence
Glasgow
United Kingdom

I.J. Taylor

University of Glasgow
School of Engineering
Glasgow
United Kingdom

R.J. Gollan

University of Queensland
School of Mechanical and Mining Engineering, Centre for Hypersonics
Brisbane
Australia

ABSTRACT

The Eddy Dissipation Model is critically analyzed with respect to the ability to address the turbulence-combustion interaction process inside scramjet engines designed to operate at high Mach numbers. The aim is to identify the most appropriate strategy for the use of the model for design purposes. To this end, three hydrogen-fueled experimental scramjet configurations with different fuel injection approaches are studied numerically. The first case consists of parallel fuel injection and it is shown that relying on estimates of ignition delay from a one-dimensional kinetics program can greatly improve the effectiveness of the EDM. The second case considers fuel injection behind a strut. Here the EDM predicts two reacting layers along the domain which are not experimentally captured from a certain distance downstream the point of injection. The last case considered a transverse injection of hydrogen and the EDM approach provided an overall good agreement with experimental pressure traces except in the vicinity of the injection location. The EDM approach appears to be a suitable tool for combustor design incorporating different fuel injection mechanisms.

[*] **jimmyjohn.hoste@strath.ac.uk**

Received DD MM YYYY; revised DD MM YYYY; accepted DD MM YYYY.

NOMENCLATURE

$\bar{a}$	$= a + a^{'}$, Reynolds average of variable a
$\tilde{a}$	$= a + a^{''}$, Favre average of variable a
$a^{'}$, $a^{''}$	fluctuating part in decomposition of a
A	Arrhenius pre-exponential constant
A_{edm}	constant of the EDM
B_{edm}	constant of the EDM
E	mixture total energy per unit mass (J/kg)
H	mixture total enthalpy per unit mass (J/kg)
I	turbulence intensity $(\%)$
J_{s_j}	diffusion flux components of species s $(kg/(m^2 s))$
k	turbulent kinetic energy (J/kg)
k_f	forward reaction rate constant
k_b	backward reaction rate constant
M	Mach number
$\dot{m}_s$	mass flow rate (kg/s)
Pr_t	turbulent Prandtl number
p	static pressure (Pa)
p_{pitot}	Pitot pressure (Pa)
q_j	heat flux components (W/m^2)
Sc_t	turbulent Schmidt number
s	mass stochiometric ratio
T	static temperature (K)
T_A	Arrhenius activation temperature (K)
T_0	total temperature (K)
t	time (s)
u_i	velocity components (m/s)
W_s	molar mass of species s (kg/mol)
X_s	molar fraction of species s
$[X_s]$	molar concentration of species s (mol/m^3)
x_j	cartesian coordinates (m)
Y_s	mass fraction of species s

Greek Symbol

β^*	$= 0.09$, turbulence model constant
δ_{ij}	kronecker delta: 0 $(i \neq j)$, 1 $(i = j)$
ϵ	dissipation of turbulent kinetic energy (m^2/s^3)
η_c	combustion efficiency
μ_t/μ	ratio of turbulent to laminar viscosity
$\nu_m^{'}$	forward stochiometric coefficient
$\nu_m^{''}$	reverse stochiometric coefficient
ρ	mixture density (kg/m^3)
$\bar{\rho}\widetilde{u_i^{''}u_j^{''}}$	Reynolds stress tensor components $(kg/(ms^2))$
τ_{ij}	molecular stress tensor components $(kg/(ms^2))$
ω	dissipation rate of turbulent kinetic energy $(1/s)$

$\dot{\omega}_s$ reaction rate of species s $(kg/(m^3 s))$

1.0 INTRODUCTION

Scramjet technology has been the subject of many studies since the late 1950s as it provides an efficient means of flying at hypersonic speeds. Potential applications include hypersonic cruise vehicles and access-to-space systems. For example, the Australian SPARTAN program aims at exploring the advantages of hydrogen-fueled scramjets by designing a three-stage-to-orbit rocket-scramjet-rocket launch system with reusable first and second stages[1,2]. As an accelerator for access-to-space, the high Mach regime ($\approx$ 7-12) at which a scramjet will operate is characterized by a combustion process which can be considered to be mainly mixing limited[3,4,5]. For design purposes, it is desirable to have a computational technique that can run effectively and efficiently account for turbulence chemistry interaction in the mixing-limited combustion process, and, subsequently, assess the overall combustor performance.

Numerical tools with different levels of fidelity are intensively used in the design of scramjets. Quasi-one-dimensional models have been developed which rely on simplified assumptions to describe the supersonic combustion process[6,7,8]. Being computationally cheap, such low-fidelity approaches are attractive for integration as a subsystem in a complete vehicle analysis as well as in Multi-disciplinary Design Optimization (MDO), but in some cases these methods may not provide a sufficient level of accuracy or consistency with the physics when complex engine configurations are considered. Steps are being taken towards the improvement of the mixing and combustion models for such low-fidelity methods by introducing surrogates informed by more accurate Computational Fluid Dynamics (CFD) approaches[9] capable of capturing the complex flow field inside scramjets and to account explicitly for the turbulence-chemistry interaction mechanisms inside the combustor section of the engine. Chemically reactive Reynolds-Averaged Navier-Stokes (RANS) still remains the most used approach when targeting design[10,11]. This is mainly related to its more manageable computational cost with respect to methods like LES (Large-Eddy Simulations) or hybrid RANS/LES which provide superior accuracy and insight into the detailed physics of the combustion mechanism but at a higher computational expense.

In the context of RANS-based approaches, the Eddy Dissipation Model (EDM) introduced by Magnussen and Hjertager[12] is a quite capable approach to address turbulence / chemistry interaction (TCI) for mixing-limited scramjets. The use of EDM in the modeling of hydrogen-fueled scramjet flows has been reported in the literature by Edwards et al.[13] using the REACTMB in-house CFD solver and it has also been largely documented in the case of commercially available software[14,15,16,17]. However, little information is found in the open literature about the optimal use of the EDM for scramjets with different types of fuel injection configurations or possible improvements of the model to increase its accuracy. This includes the specification of model parameters for which no consistent guidelines are available, and for which details are typically not communicated.

The aim of the present work is to elaborate on the capability of the EDM in addressing supersonic mixing-limited combustion processes with a focus on the overall design process

of the combustor under the perspective of potentially introducing such approach within MDO frameworks. The optimal use of the model is inferred for three specific scramjet combustors that conceptually represent the most relevant configurations based on different fuel injection and shock wave pattern schemes.

The paper is structured as follows. In Section 2, the RANS equations for turbulent reacting flows are presented as well as the detailed formulation of the EDM. Section 3 describes the scramjet test cases used in this work followed by the results of the simulations. A critical discussion summarizing the results is presented in Section 4. Final remarks and proposed future directions are reported in Section 5.

2.0 NUMERICAL MODELING

The governing equations for turbulent compressible reacting flows can be written as

Mass Conservation:

$$\frac{\partial \bar{\rho}}{\partial t} + \frac{\partial}{\partial x_i}\left(\bar{\rho}\tilde{u}_i\right) = 0 \qquad \ldots(1)$$

Momentum Conservation:

$$\frac{\partial}{\partial t}\left(\bar{\rho}\tilde{u}_i\right) + \frac{\partial}{\partial x_j}\left(\bar{\rho}\tilde{u}_j\tilde{u}_i + \delta_{ij}\bar{p}\right) = \frac{\partial}{\partial x_j}\left(\bar{\tau}_{ji} - \bar{\rho}\widetilde{u_i'' u_j''}\right) \qquad \ldots(2)$$

Energy Conservation:

$$\frac{\partial}{\partial t}\left(\bar{\rho}\tilde{E}\right) + \frac{\partial}{\partial x_j}\left(\bar{\rho}\tilde{u}_j\tilde{H}\right) = \frac{\partial}{\partial x_j}\left(\bar{\tau}_{ij}\tilde{u}_i + \overline{\tau_{ij}u_i''} - \bar{q}_j - \bar{\rho}\widetilde{H'' u_j''}\right) \qquad \ldots(3)$$

Species Conservation:

$$\frac{\partial(\bar{\rho}\tilde{Y}_s)}{\partial t} + \frac{\partial(\bar{\rho}\tilde{Y}_s\tilde{u}_j)}{\partial x_j} = \bar{\dot{\omega}}_s - \frac{\partial}{\partial x_j}\left(\bar{J}_{s_j} + \bar{\rho}\widetilde{Y_s'' u_j''}\right) \qquad \ldots(4)$$

with conserved variables $\bar{\rho}$, $\bar{\rho}\tilde{u}_j$, $\bar{\rho}\tilde{E}$, $\bar{\rho}\tilde{Y}_s$ representing density, momentum, total energy per unit volume and partial densities of the species s (s=1,...,N). Throughout this work, the above set of equations will be referred to as the Reynolds Averaged Navier-Stokes equations (RANS). The symbols $\bar{x}$ and $\tilde{x}$ denote respectively the time and Favre (or density-weighted) average. Equations (1) to (4) are written in such a way that those terms which require modeling are indicated on the right-hand side. The system of conservation equations for a turbulent chemically reacting flow needs extensive modeling. A comprehensive overview of the modeling practice for supersonic internal flows can be found in the work of Baurle[10]. The present work will only address the treatment of the mean species reaction rates $\bar{\dot{\omega}}_s$.

In this work, the RANS equations are solved with the Eilmer[18] open-source CFD package, developed at the University of Queensland. The finite volume solver addresses turbulence closure by means of Wilcox's 2006 $k-\omega$ model[19] and has been previously validated for scramjet type flows[20,21,22]. Shock capturing is ensured by treating the inviscid fluxes with an adaptive method switching between Macrossan's Equilibrium Flux Method (EFM)[23] and

Liou and Wada's AUSMDV[24]. With its more diffusive character, the former is active in regions with strong gradients in velocity while the latter is used elsewhere. Viscous fluxes are treated by means of Gauss' theorem and the forward Euler scheme or a predictor-corrector scheme (Heun's method) is used for the time integration. Eilmer[25] adopts temperature dependent species heat capacities and energies that are evaluated with the polynomial curve fits of McBride and Gordon[26]. The main modeling issue in high-speed turbulent reacting flows is the chemical source term ($\bar{\dot{\omega}}_s$) which is highly non-linear and cannot be directly related to mean flow properties. It is the role of the TCI model to specify this source term. In the following subsection the assumptions of the EDM are introduced followed by the expression for ($\bar{\dot{\omega}}_s$). Thereafter, the limitations of the model are outlined.

2.1 Physical interpretation of the Eddy Dissipation Model

The Eddy Dissipation Model (EDM) was introduced by Magnussen and Hjertager[12,27]. It assumes that fuel and oxidizer are carried by separate eddies in diffusion flames. Furthermore, chemical reactions are fast so that fuel and oxidizer will react as soon as they mix on a molecular scale. Assuming this fast chemistry limit in the EDM, the rate at which reactions occur is then dependent on the rate at which turbulent eddies carrying fuel and oxidizer are brought together. In other words, the mean reaction rate is mainly controlled by a turbulent mixing time. On dimensional basis, this mixing time is estimated from the integral length scales by using the turbulence model parameters which describe the energy cascade process in turbulent flows. Consequently, the mixing on a molecular level is dependent on the rate at which the eddies dissipate. The model is sometimes referred to as "mixed-is-burned" which highlights the idea that once fuel and oxidizer is considered mixed, it burns immediately (fast chemistry).

2.2 Implementation of the Eddy Dissipation Model

The EDM is implemented by assuming a single-step irreversible reaction of the form $\nu_F^{'} F + \nu_O^{'} O \rightarrow \nu_P^{''} P$, where ν_s are the stoichiometric coefficients of Fuel (F), Oxidizer (O) and Products (P). Such a form is consistent with the model's physical description of fast-occurring chemical reactions. It must be noted that the model is limited to scramjet configuration where the chemical time scales are much smaller with respect to the turbulent time scales and is believed to be the case at high Mach regimes. The use of a single-step irreversible reaction instead of a reaction mechanism reduces the computational cost and makes it useful for design. In the case of hydrogen combustion, the reaction is :

$$2H_2 + O_2 \rightarrow 2H_2O \qquad \ldots(5)$$

and N_2 acting as an inert species, resulting in four species equations (Equation 4). In EDM, the reaction rate of fuel is defined as:

$$\bar{\dot{\omega}}_F = -A_{\text{edm}}\, \bar{\rho}\beta^* \omega \min\left[\tilde{Y}_F, \frac{\tilde{Y}_O}{s}, B_{\text{edm}}\frac{\tilde{Y}_P}{s+1}\right] \qquad \ldots(6)$$

The oxidizer and product reaction rates can then be obtained as:

$$\bar{\dot{\omega}}_O = s\, \bar{\dot{\omega}}_F \quad , \quad \bar{\dot{\omega}}_P = -(s+1)\bar{\dot{\omega}}_F \qquad \ldots(7)$$

In the above equation s is the mass stoichiometric ratio defined as $s = (\nu'_O W_O)/(\nu'_F W_F)$ and equals 8 for H_2-air combustion. W_s is the molar mass in kg/mol and $\tilde{Y}_s$ the mass fraction. In Equation 6, β^* is a turbulence model constant with a value of 0.09 and ω (1/s) is the specific dissipation of turbulent kinetic energy obtained through the turbulence model. The underlying physical assumption regarding the dissipation of turbulent eddies in the model is accounted for through the latter parameter.

2.3 Specification of the model constants

A_{edm} and B_{edm} are model constants which have standard values of 4.0 and 0.5. This combination of values follows from the work of Magnussen and Hjertager[12]. In the study of six different low-speed flame simulations, in conjunction with the k-ϵ turbulence model, satisfactory results in comparison with experimental data were obtained by adopting these standard values. However, this combination might not be the most appropriate for scramjet flow fields. Edwards et al.[13] suggest a value for A_{edm} between 1 and 4. The physical effect of increasing this constant's value is the promotion of the turbulent eddy dissipation process in the flow field which, where available, brings fuel and oxidizer together on a molecular level. In summary, the mean fuel reaction rate of EDM, $\bar{\dot{\omega}}_F(kg/(m^3.s))$, is a function of turbulence (ω), and the mass fractions of fuel ($\tilde{Y}_F$), oxidizer ($\tilde{Y}_O$) and products ($\tilde{Y}_P$) in every cell of the domain. Note that the latter term in the minimum evaluation of Equation 6 is intended to account for the effect of hot (or cold) products in a premixed turbulent flame situation where both fuel and oxidizer are contained within the same eddies[12]. The importance of the products on the combustion process can be controlled through the parameter B_{edm}. An increase in value of B_{edm} will promote the reaction between fuel and oxidizer as more hot products are present to ignite the premixed mixture. The premixed situation is not very common in scramjet flows except for the case of oxygen enrichment. Moreover, the inclusion of the product term implies that for reactions to occur an initial product mass fraction is required. This value is usually taken as 0.01. This work does not consider the product term.

2.4 Limiting the reaction rate within EDM

The EDM does not include any effect of finite-rate chemical kinetics. Equation 6 does not account for the temperature on the formation of products. Consequently, the EDM has a tendency to over-predict the fuel consumption as well as peak temperatures. The way to mitigate these disadvantages is by limiting $\bar{\dot{\omega}}_F$ with a kinetic reaction rate. This can be done by use of the reaction rate obtained with the "no-model" or Arrhenius approach (law of mass action) and a single step global reaction[10]:

$$\bar{\dot{\omega}}_F = \min(\bar{\dot{\omega}}_{F,\text{edm}}, \bar{\dot{\omega}}_{F,\text{lam}}) \quad \ldots(8)$$

where $\bar{\dot{\omega}}_{F,\text{lam}}$ is given by:

$$\bar{\dot{\omega}}_{F,\text{lam}} = -\nu'_F W_F \left[k_f [X_F]^{\nu'_F} [X_O]^{\nu'_O} - k_r [X_P]^{\nu'_P}\right] \quad \ldots(9)$$

The kinetic limit allows the extension of the EDM's applicability to test cases where the combustion is not purely mixing limited but where ignition delay effects are present.

However, the trade-off is the introduction of two reaction rate parameters which are not universally defined: the forward reaction rate k_f and the backward or reverse reaction rate k_r. The former is obtained with Arrhenius law by defining a pre-exponential constant A and an activation temperature T_A for a single step global reaction of the hydrogen-air combustion. Several options are available in the open-literature for the Arrhenius law constants and this work will adopt the values A=1.1e19 and T_A = 8052 K as proposed by Chandra Murty and Chakraborty[15]. These values have been obtained for hydrogen combustion by requiring that the flame speed of the single step kinetics match with those from full chemistry as pointed out by Sekar and Mukunda[28]. The k_r is obtained from the forward rate and equilibrium constant. The use of Equation 8 will be referred to as "EDM with kinetic limit". $[X_s]$ is the molar concentration in this definition. As pointed out by Baurle[10], the use of EDM does alleviate the stiffness of the governing equations as turbulent time scales are driving the reactions. This characteristic makes the use of EDM beneficial for design purposes.

In the case of non-premixed scramjet flow path simulations with EDM, on top of the model constant A_{edm}, values for turbulent Prandtl (Pr_t) and Schmidt number (Sc_t) have to be specified. Including the possibility to limit reaction rates with a kinetic limit, this leaves the user to specify a combination of 3 (or 4) parameters per simulation. Details about the settings and effect of parameter values choices are presented in the following sections.

3.0 TEST CASES

Three generic scramjet combustor geometries are selected to study the most appropriate use of the EDM, each with a different fuel injection arrangement. The assessment is based on the predictive capability of the model by comparison with available experimental data. The first test case is the experiment of Burrows and Kurkov[29,30] (Figure 1) where hydrogen is injected parallel to a vitiated air-stream behind a backward facing step. The experimental design results in high combustor entrance Mach number (> 2) and static temperature (> 1000 K), typical for high flight Mach numbers. A mixing layer is generated close to the injection and a runaway length is observed where the fuel and oxidizer mix before igniting. Whilst the ignition delay is kinetically controlled, it will be demonstrated that once the flow ignites the combustion is mixing limited. The second test case is the DLR combustor experiment of Waidmann et al.[31] (Figure 12). In this case, hydrogen is injected behind a strut. The physics inside the combustor is dominated by a pattern of shock waves interacting amongst themselves and with shear layers. Turbulence modeling will play a crucial role in capturing the mixing layers and recirculation regions generated behind the strut. These physical features are, in turn, key in controlling the behavior of the flame held behind the strut and the transport of the species along the combustor. A Mach 2 vitiated air stream is supplied to the test chamber with cold temperature (< 1000 K) due to limitations of the facility. Most of the studies reported in the literature on this configuration adopt a TCI which assumes that turbulent time scales are larger than chemical time scales. Waidmann et al.[31] identified the combustion mode to be situated in the flamelet regime. This an indication that, in spite of the cold vitiated air stream conditions, the combustion process is primarily mixing limited. The flamelet and EDM commonly rely on the assumption of that chemical time scales are smaller than mixing time scales. The DLR combustor is therefore adequate for the study of the EDM in this work. The third test case is the HyShot II combustor[32,33], ground tested at DLR,

where fuel is injected perpendicular to the incoming flow inside the constant area combustor. Similar to the experiment of Burrows and Kurkov, the entrance Mach number (> 2) and static temperature (> 1000 K) are representative for a high flight Mach number. It was demonstrated in several RANS studies[33,34] that the combustion is primarily mixing limited. Moreover, the same comment was made by Larsson et al.[35] in their numerical study of the combustor with LES. The HyShot II combustor is therefore a suitable candidate for study with the EDM. The selected test cases are characterized by different physical features which is suitable for assessing a model's predictive capability over a broader range of supersonic combustion phenomena.

Unit Lewis number is assumed for each species throughout this work and in the case of viscous walls without wall functions, the value of ω is set according to Menter's suggestion for smooth walls[36]. A CFL value of 0.5 is adopted for time integration using the Euler or predictor-corrector scheme. Simulations are converged to a steady state and convergence is monitored through point probes of velocity, density, temperature and pressure at different locations in the computational domains.

3.1 Case 1: Burrows-Kurkov

A commonly used test case in CFD code validation studies for supersonic combustion is the experiment of Burrows and Kurkov[29,30] (BK) shown in Figure 1 for which an extensive set of comparison data in pure mixing and reacting conditions is available. Many authors have performed RANS studies of the geometry over the last three decades including[37,38,39,40,41,42,43]. The test case is known to be very sensitive to the the values of turbulent Prandtl (Pr_t) and Schmidt (Sc_t) numbers. Following a sensitivity study for Wilcox k-ω 2006 model, it was observed that the combinations $Pr_t = 0.9$, $Sc_t = 0.5$ and $Pr_t = 0.5$, $Sc_t = 0.5$ gave very similar results in comparison with the experimental data at the exit of the combustor. Simulations with the latter combination are presented here.

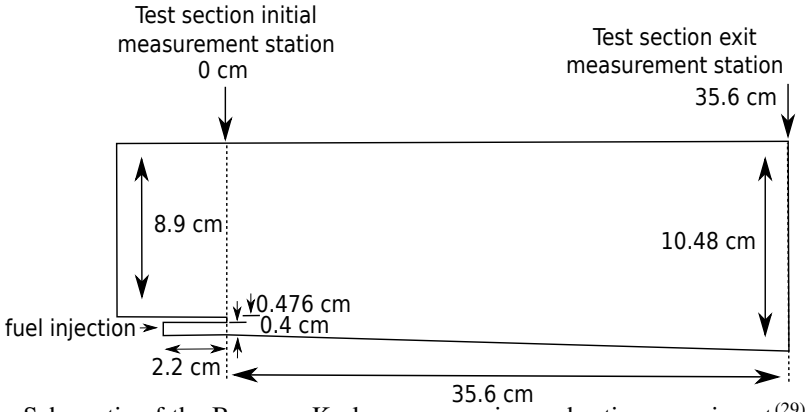

Figure 1: Schematic of the Burrows-Kurkov supersonic combustion experiment[29]. Not to scale.

3.1.1 Problem Formulation

The experimental setup in Figure 1 has been simulated in two stages. In the first stage, a boundary layer section (BLS) of 65 cm is considered using the same vitiated air supersonic inflow conditions as Edwards et al.[44] listed in Table 1. Note that these values differ from the ones typically encountered in the literature, however Edwards et al.[44] demonstrated a very good agreement overall with experiments in their work. Values for turbulence intensity (I) and the ratio of turbulent to laminar viscosity (μ_t/μ) are set to 5 % and 10 respectively. The exit profile of the first stage is used as an inflow condition for the second stage which considered the geometry depicted in Figure 1 with a BLS of 2 cm. The injector is simulated as a constant area channel of 2.2 cm with conditions in Table 1. Turbulence boundary conditions for the injector are the same as for the separate BLS simulations. Walls are treated as isothermal at a temperature of 300 K. A supersonic outflow is prescribed where values from the interior of the domain are extrapolated. The simulation results in terms of profiles of total temperature and Pitot pressure are depicted in Figure 2. The profiles are compared to the experimental data collected at the first section (x = 0 cm) as well as to the CFD of Edwards et al.[44] obtained with a hybrid RANS / LES approach. An overall satisfactory prediction of the inflow conditions are observed with a boundary layer thickness at the entrance of the combustor around 1 cm.

Table 1: Inflow and injector flow conditions for Burrow-Kurkov' experiment.

	inflow	injector
u (m/s)	1741.4	1217.0
T (K)	1237.9	254.0
p (Pa)	96000.0	101350.0
Y_{H_2} (-)	0.0	1.0
Y_{O_2} (-)	0.258	0.0
Y_{H_2O} (-)	0.256	0.0
Y_{N_2} (-)	0.486	0.0

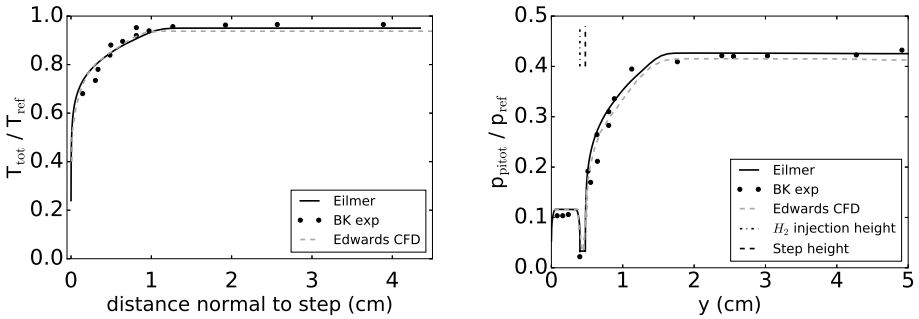

(a) (b)

Figure 2: Vitiated air flow total temperature (a) and Pitot pressure (b) at the entrance of the combustor. T_{ref}=2380 K, p_{ref}=17.1e5 Pa

For the second stage calculation, a mesh independence study has been performed with structured grids containing 129 987 (mesh 1) and 185 920 (mesh 2) cells. In both cases, the maximum first cell distance to physical walls was below 5e-6 m. The EDM with setting A_{edm} = 4 was adopted. The result of the mesh refinement study on the total temperature (T_0) at the exit of the combustor (x = 35.6 cm) is shown in Figure 3. The horizontal axis represents the distance from the lower wall. No visible differences in predictions are observed indicating mesh independent results. The same is valid for the combustion efficiency along the combustor. This paramater has been computed according to Kim et al.[45] as :

$$\eta_c(x) = 1 - \frac{\int \rho u Y_F dA}{(\int \rho u Y_F dA)_{x=0}} = 1 - \frac{\dot{m}_F}{(\dot{m}_F)_{x=0}} \quad \ldots(10)$$

Equation 10 evaluates the mass flow rate of fuel ($\dot{m}_F$) across a plane at any position with respect to the injected amount. The profiles of η_c obtained by both meshes are very similar and a mesh independent result is achieved. In the following discussion the finer mesh is considered.

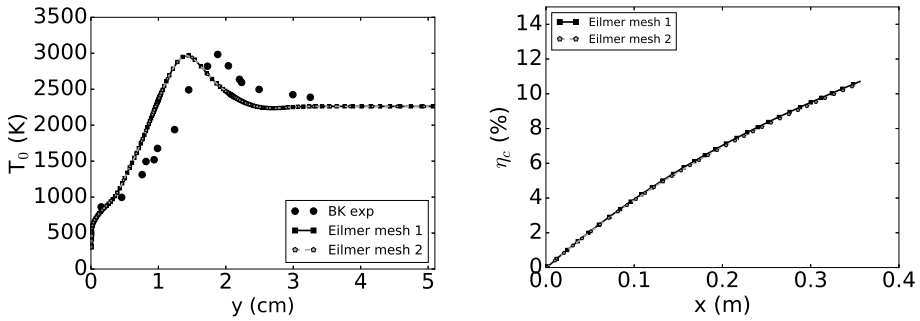

(a) (b)

Figure 3: Predictions of total temperature at x=35.6 cm (a) and combustion efficiency (b) obtained with different mesh sizes.

3.1.2 Results

The influence of the A_{edm} parameter is assessed through comparison with the available experimental data measured at the exit plane (x= 35.6 cm) in Figures 4 to 7. The horizontal axis represents the vertical distance from the lower wall. Simulations have been performed with several values of the A_{edm}. No kinetic limit has been used in these results. It will be shown hereafter that it did not influence the different profiles at the exit of the test section.

The effect of varying A_{edm} is observed in the profile of total temperature (T_0) in Figure 4. A higher peak value is coupled to a higher A_{edm} setting. This behavior is a direct consequence of the model (Equation 6) as more products are allowed to be formed which in turn relates to an increased mean temperature. A value of 6 results in a peak value comparable to experiments,

however the location is closer to the lower wall by ≈ 0.44 cm (4.2 % of the exit height). An increase of the standard setting of $A_{edm} = 4$ does not demonstrate drastic changes which suggests the presence of an asymptotic limit. This can be explained by the scarce presence of reactants still available for reaction at that location predicted by the EDM (Figure 7, y ≈ 1.5 cm). Experimentally this situation occurs further away from the wall. Adopting a lower value of the model constant ($A_{edm} = 1$) results in a consistent under-prediction of the peak total temperature. Regarding the profiles of Mach number, a higher A_{edm} setting is in better agreement with the experimental data. Overall a good match with experiment is observed for Mach number. Figure 5, showing Pitot pressure (p_{pitot}) and mass flow, confirms the need for a higher value of the EDM constant in order to get an improved agreement with experiments. The influence is, however, contained to the region closer to the wall (y < 2 cm).

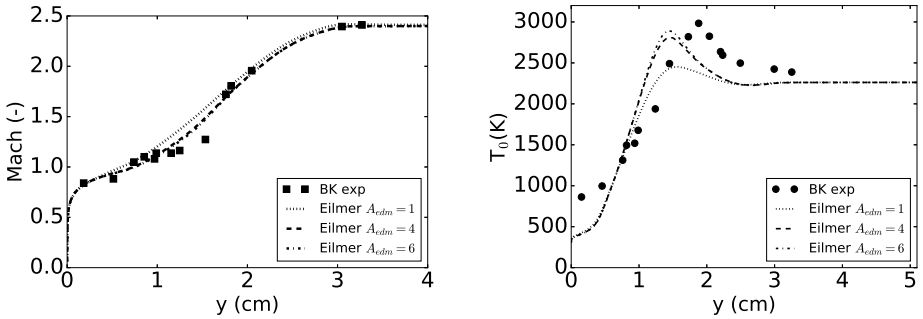

(a) (b)

Figure 4: Predictions of Mach (a) and total temperature (b) at x=35.6 cm obtained with EDM compared with experimental values of Burrows and Kurkov.

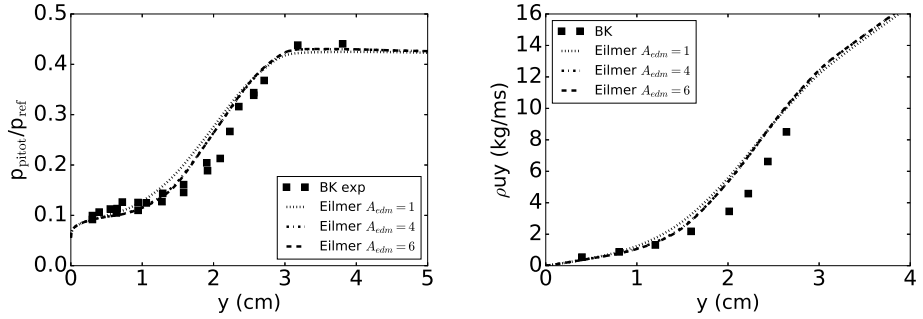

(a) (b)

Figure 5: Predictions of Pitot pressure (a) and mass flow (b) at x=35.6 cm obtained with EDM compared with experimental values of Burrows and Kurkov. P_{ref}=17.1e5 Pa

Figures 6 and 7 show the exit profiles of species mole fractions. The observations on the effect of A_{edm} on the H_2O mole fraction are in agreement with the total temperature curves

discussed previously. A higher setting predicts peak values comparable to experiment but an offset in peak position is present. The different EDM results under-predict the penetration depth of hydrogen into the vitiated airflow. The X_{O_2} profiles show that the experimental slope is better captured by a higher value of the EDM constant.

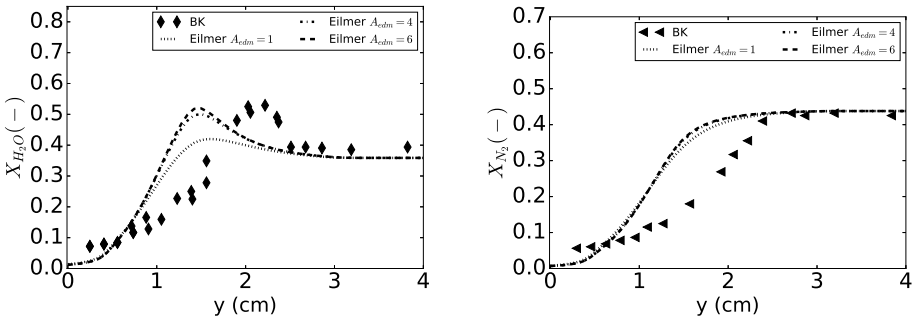

(a) (b)

Figure 6: Predictions of H_2O (a) and N_2 (b) mole fraction at x=35.6 cm obtained with EDM compared with experimental values of Burrows and Kurkov.

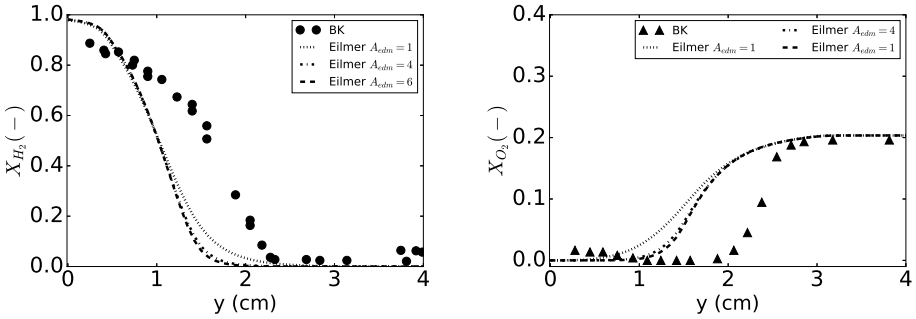

(a) (b)

Figure 7: Predictions of H_2 (a) and O_2 (b) mole fraction at x=35.6 cm obtained with EDM compared with experimental values of Burrows and Kurkov.

Overall the best results with EDM are obtained by prescribing $A_{edm} = 6$. The explanation for this can be understood by studying the contour of product mass fraction $Y_P = Y_{H_2O}$ (or mean temperature) and ω. Figure 8 shows the product mass fraction contour predicted by the EDM (upper representation). The contour is in accordance with what would be obtained with a single-step reaction (see[46]) except for the fact that combustion occurs very close to the injection point. This behavior, which is unphysical, is expected as the EDM allows products to be formed as soon as fuel and oxidizer mix. Introducing the kinetic limit (Equation 8) does mitigate this effect as can be seen in the bottom contour. It was mentioned earlier that applying this limit does not affect the CFD predictions at the exit of the combustor. This

statement is confirmed by observing the profiles of Mach number and total temperature in Figure 9. The same observations are valid for the other quantities and are therefore not shown in this work. The kinetic limit only affects a very small region near the injector and the length of the combustor is long enough so as to allow the EDM to compensate this localized effect near the injector. The minimal influence of the kinetic limit is explained by the high vitiated air-stream temperature. In the experiments, ignition onset is indicated by a rise in wall static pressure 18 cm downstream the injection point[30]. With the kinetic limit this occurs at ≈ 1 cm downstream the same injection point.

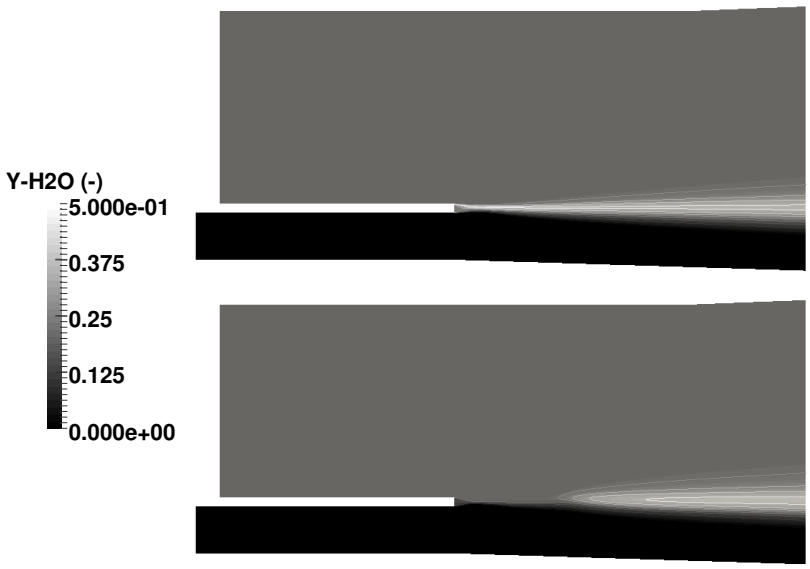

Figure 8: Mass fraction contours of H_2O close to the injection point with from top to bottom: EDM, EDM with kinetic limit.

The EDM assumes that a high rate of mixing is characterized by a high value of ω. This assumption is not valid near the injector where no combustion is taking place but where very high values of ω are predicted by the turbulence model in Figure 10. Moving further away from this point a decrease in ω is observed which is coupled to a decay in the strength of the turbulence inside the combustor. The high local values in the shear layer near the injector is the cause for an early product formation given the direct influence of ω in Equation 6 and the availability of both fuel and oxidizer. In reality the combustion should start after some ignition delay. The location for ignition onset is downstream of the injection point where the value of omega decreases. Consequently, an increase in the A_{edm} constant is required as a compensation. Values much higher than 6 have no strong influence as there are not enough reactants at stochiometric ratio left to burn at the interface between fuel stream and the vitiated air stream.

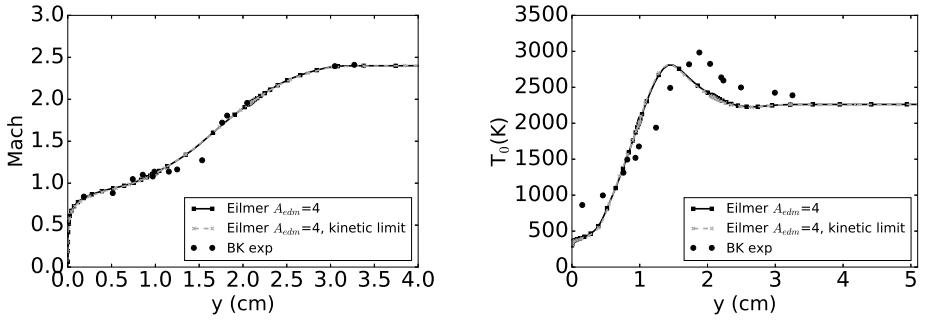

(a) (b)

Figure 9: Comparison of EDM with and without kinetic limit on Mach (a) and total temperature (b) at the exit of the combustor (x = 35.6 cm)

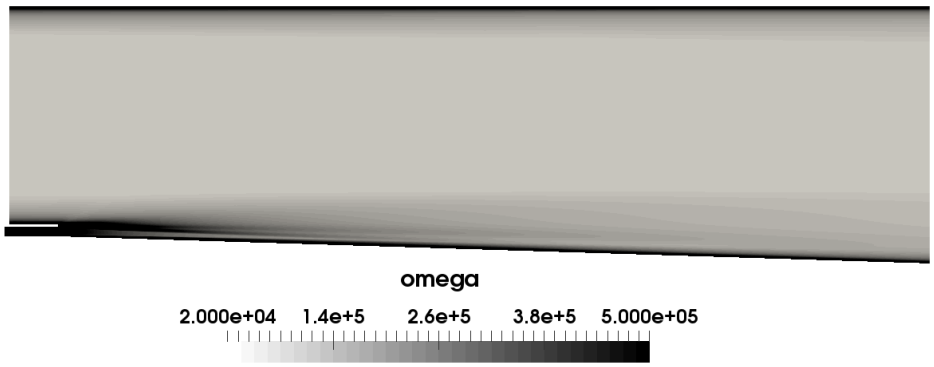

Figure 10: Contour of ω for the experiment of Burrows and Kurkov

Ignition Delay with Zonal EDM

Figure 8 demonstrates that the kinetic limit is perhaps not the most adequate way of introducing an ignition delay in a shear layer environment with high free stream temperature. Moreover, the combustion induced shock wave, reported by Bhagwanding et al.[46], is not predicted by the EDM. The reference work of Burrow and Kurkov[29] mentions that it is possible to rely on a one-dimensional kinetics program to obtain an estimate of the expected ignition delay. Such an approach can very very beneficial for the use of the EDM, which lacks the ability to account for ignition delay in a parallel injection setting with high free stream temperatures (above autoignition of hydrogen), as shown here. Based on a free stream temperature of 1270 K, an H_2/O_2 ratio of 0.013 and a free stream mixture containing N_2, O_2, H_2O and NO, an induction time (or ignition delay or runaway length) of 90e-6 s was obtained[29] with the one-dimensional kinetics program developed by Bittker and Scullin[47]. Using an averaged vitiated air stream velocity at the entrance of the combustor of 1689 m/s (obtained from CFD), a flow length equal to 2.1e-4 s is obtained. The latter value yields an estimate of a fluid element residence time inside the combustor. From this value and the previously calculated induction time, the ignition location inside the combustor is

estimated to be at x = 0.153 m. Note that this approach only gives a rough estimate of the induction process. It does, for example, not account for the low fuel stream temperature near the wall which can have a significant influence as indicated by Burrows and Kurkov[29]. Nevertheless, this information can be relied on for a better use of the EDM. A similation has been performed relying on the above estimate where no combustion is allowed at any axial location before that point, hence the terminology "zone". Recall that experimentally[30] an ignition delay is observed between 18 (wall pressure trace) and 25 cm (photographs of OH radiation). Numerical predictions have also been obtained with a finite-rate chemistry simulations (no TCI) relying on the 7 species, 8 reactions mechanism of Evans-Schexnayder (E-S)[37] with modified third-body efficiencies in accordance with Bhagwandin et al.[46]. The finite rate chemistry (FRC) simulation with the latter mechanism predicted an onset of ignition at a position of 23 cm.

Figure 11 compares the different approaches with experimental values of Mach number and total temperature (T_0) at the combustor exit. The classical EDM is shown for a constant value $A_{edm} = 6$ following the parametric study discussed previously. The profiles of T_0 show that the use of the EDM can be greatly improved with an estimate of ignition onset. A very good agreement with experimental T_0 values are observed near the wall with the zonal use of the EDM. The FRC (E-S) does perform better than the classic EDM but slightly less than the zonal EDM. This is explained by the fact that the combustion process is kinetically limited until the onset of ignition whereafter it becomes mixing limited. The same observation was made by Kirchhartz et al.[48] in an axisymmetric scramjet combustor with similar fuel injection mechanism. The EDM assumes a mixing limited combustion and is therefore more appropriate once the flow is ignited. In terms of the Mach number profile, a lesser agreement with experimental data is observed for the EDM with ignition estimate compared to the curve without. Nevertheless, it remains superior to the FRC CFD prediction in the vicinity of the wall.

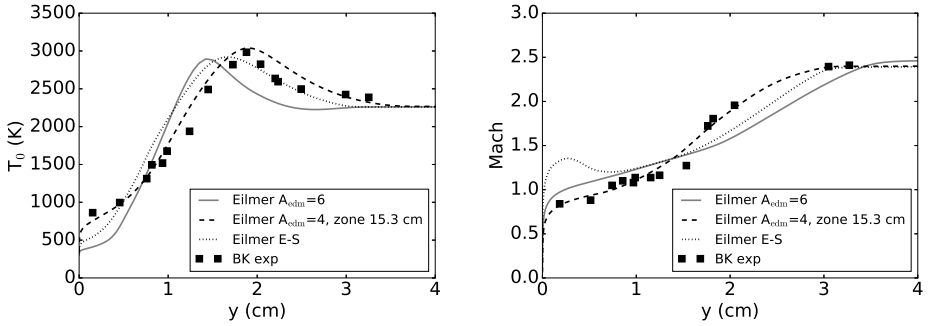

(a) (b)

Figure 11: Comparison of EDM with and without zone on total temperature (a) and Mach number (b) at the exit of the combustor (x = 35.6 cm).

In conclusion, even though the estimated induction length from the one-dimensional pro-

gram does not agree with experimental observations †, it proves to be very useful information for an improved use of the EDM. The observations in Figure 11 demonstrate that the zonal EDM provides a good estimate of the reaction zone. Therefore, the EDM with ignition delay via zonal application proves to be a viable approach to design scramjet combustors with fuel injection parallel to the air stream as opposed to ignition delay with the kinetic-limited rate.

3.2 Case 2: DLR combustor

The DLR combustor experiment of Waidmann et al.[31] is depicted in Figure 12. Similar to the Burrows-Kurkov experiment, measurements have been taken in both a pure mixing and a combusting setting. The main geometry is notionally two-dimensional, however the use of porthole injectors on the rear of the strut sets up an inherently three-dimensional flow field. Several two-and three-dimensional RANS studies of this combustor test case can be found in the literature[49,50,16,51,52,53] where each author introduces a TCI model. In spite of the three-dimensionality of the configuration, two-dimensional studies are useful as a proof of concept for modeling techniques. Oevermann[49] and Mura et al.[50] obtained reasonable results in their two dimensional studies. Following this approach, the present work considers the application of EDM on a two-dimensional domain with single slot injector. It is expected that the two-dimensional assumption will introduce a certain degree of error when making direct comparison to experiment.

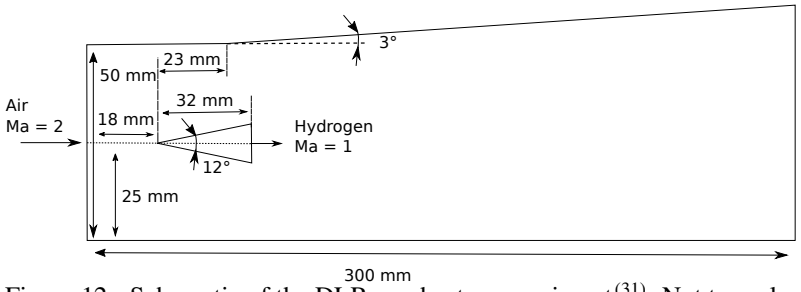

Figure 12: Schematic of the DLR combustor experiment[31]. Not to scale.

3.2.1 Problem Formulation

A structured grid has been generated for the domain shown in Figure 12. The distance between the supersonic inlet, with conditions given in Table 2, and the start of the strut is taken as 18 mm and the total combustor length as 300 mm. Upper and lower walls are treated as inviscid which is an acceptable choice given the distant location with respect to the reaction zone. The strut walls are defined as adiabatic and supersonic outflow is assumed. Given the relatively low stream temperatures in the combustor and the location of the reaction zone further downstream of the strut, the heat transfer to the strut walls is expected to be small supporting the adiabatic wall boundary condition setting. Turbulence quantities are

† It must be noted that the BK test case is very sensitive to the selected turbulence model[40], inflow conditions[40] and reaction mechanism[46]. Moreover, there is some uncertainty regarding the onset of ignition.

taken similar to Oevermann[49] and Mura et al.[50]: for the free stream inflow $I = 0.3\%$, $\mu_t/\mu = 675$ and for the injector $I = 3.3\%$, $\mu_t/\mu = 63$.

Table 2: Inflow and injector flow conditions for the DLR combustor experiment.

	inflow	injector
u (m/s)	730.0	1200.0
T (K)	340.0	250.0
p (Pa)	100000.0	100000.0
Y_{H_2} (-)	0.0	1.0
Y_{O_2} (-)	0.232	0.0
Y_{H_2O} (-)	0.032	0.0
Y_{N_2} (-)	0.736	0.0

A mesh independence study has been performed with structured grids containing 117 000 (mesh 1) and 276 432 (mesh 2) cells. For this study, the EDM with setting A_{edm}=4 and a combination $Pr_t = Sc_t = 0.9$ was adopted. The result is shown in Figure 13 for the horizontal velocity component along a line superimposing the symmetry axis of the strut. In the following discussions the term centerline velocity will be used instead. Some small differences are observed in the recirculation regions behind the strut (x ≈ 70 mm) as well as further downstream in the combustor. However, for most of the profile both meshes predict the same centerline velocity. Also shown in Figure 13 is the combustion efficiency computed with Equation 10. The profiles are very similar with a maximum difference of 1.5 % between the grids. Given the limited effect of the refinement (≈ factor 2) on the solution, the coarser mesh is suitable to study the application of the EDM on the combustor. Therefore the following discussion considers the first mesh.

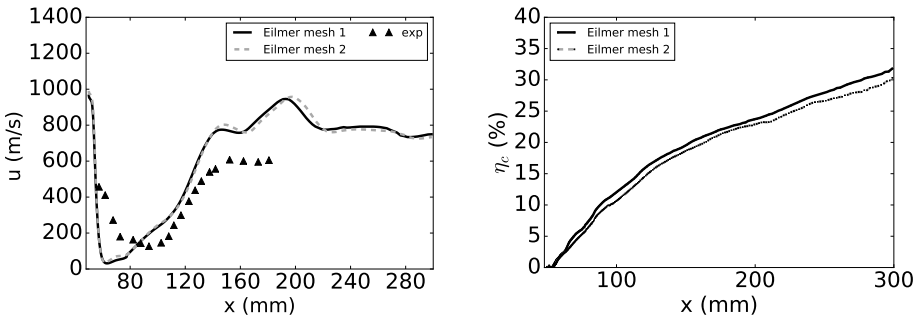

(a) (b)

Figure 13: Predictions of centerline velocity (a) and combustion efficiency (b) obtained with different mesh sizes.

3.2.2 Results

The DLR combustor test case has proven to be very challenging to predict in a two-dimensional context. Multiple combinations of the different settings were explored and only a limited number of results will be discussed in this paper. Waidmann et al.[31] collected, inter alia, data on axial velocity and temperature at the cross-sections marked with 1 and 2 in Figure 14. Firstly the effect of introducing a kinetic limit on the EDM reaction rate has been explored. Figure 15 shows its influence compared with some of the available experimental data for the EDM setting, $A_{edm} = 4$, and a turbulent setting in accordance with Gao et al.[51] of $Pr_t = Sc_t = 0.9$. Simulations with kinetic limit were initiated from the converged EDM result without limit as to avoid the need for a source of ignition given the low free-stream temperatures.

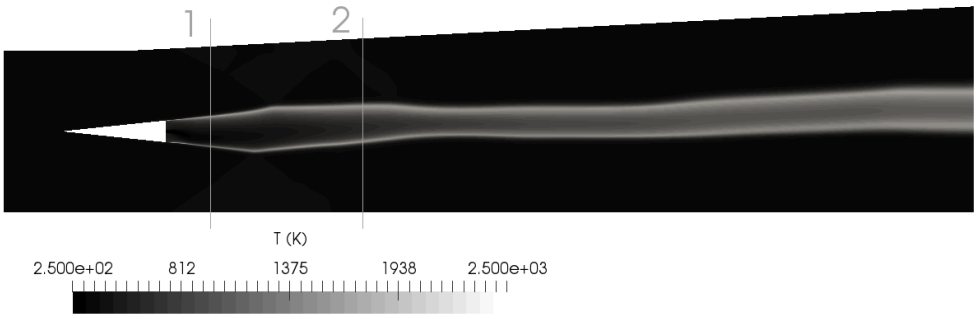

Figure 14: Temperature contour ($A_{edm} = 4$,$Pr_t = Sc_t = 0.9$) with indication of the axial measurement locations considered in the present work.

Profiles of axial velocity did not show significant differences however the temperature profiles did. This behavior can be observed in Figure 15 (b) where the axial velocity is presented at the second measurement location of Figure 14. Applying the kinetic limit mostly affected the local minimum in axial velocity between the two shear layers but its position is not influenced by the modeling option. According to the experimental measurements, the minimum around 180 m/s with kinetic limit is an under-prediction of the expected value. On the other hand, the minimum value without any limiting factor slightly over-predicts the experimental observations. Despite having similar minimum locations, the velocity profiles of the simulation are not aligned with experimental trend. It must be noted that even the more advanced CFD models[54,55,56] do not yield a good agreement with this particular set of experimental data which demonstrates the challenging nature of the test case.

The numerical results of the axial temperature profile are strongly influenced by the kinetic limit. Predictions at the first measurement station shown in Figure 14 are presented in Figure 15 (a). Applying the kinetic limit does suppress combustion in the lower recirculation region just downstream of the strut. This in turn results in a single temperature peak and is not in agreement with the experimental data. The observation is explained by the low free stream temperature and the asymmetry in the geometry. The EDM results in peak temperature

locations similar to experiments and the reference CFD. The structure of the recirculation regions are however different in the numerical simulation. Figure 15 (c) shows the centerline velocity. The end of the strut is located at x = 64 mm in this representation. As mentioned above, the structure of the recirculation regions behind the strut are different depending on whether EDM is used with a kinetic limit or not. The upper recirculation zone does extend down to the centerline which is not experimentally observed, neither predicted by the standard EDM. Further downstream inside the combustor, the profile of velocity of the EDM with kinetic limit is in better agreement with the experimental data than the other profiles. As the influence of this limit in the region close to the strut results in worse agreement with the experimental data, the kinetic limit is not applied in the following discussion.

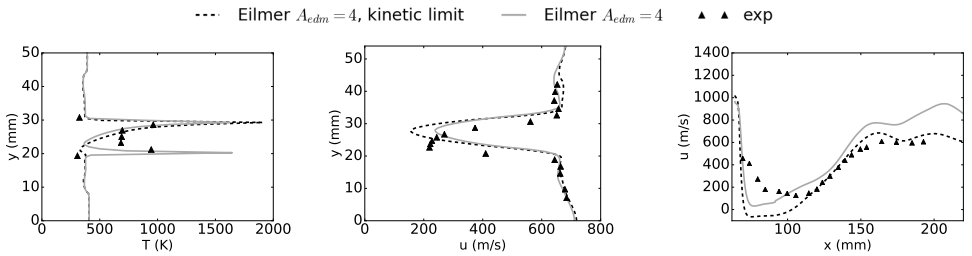

(a) (b) (c)

Figure 15: Effect of applying the kinetic limit on the temperature at axial location 1 (a), the velocity at axial location 2 (b), the centerline velocity (c). A_{edm} = 4, $Pr_t = Sc_t = 0.9$.

Secondly, the most appropriate setting for the A_{edm} constant is now investigated. From the observations in the Burrows-Kurkov test case, the configuration is expected to have very high values of ω in the shear layers induced by the strut with decreasing strength towards the end of the combustor. Figure 18 confirms this statement. Moreover, the higher ω values are as well present near the fuel injector. Experimentally, the flame is located in the vicinity of the injection point behind the strut. In contrast to Burrows-Kurkov, there is no significant runaway length. In terms of the EDM, given the high ω values behind the strut, a relatively low value of A_{edm} should be an appropriate choice. Too low a value would however negatively influence the combustion zone further downstream characterized by lower ω values. Figure 16 shows the mean temperature at locations 1 and 2 depicted in Figure 14 as well as along the lower combustor wall obtained with the same three settings of the EDM as in Burrows-Kurkov, namely A_{edm}= 1, 4 and 6. Figure 17 presents the velocity at the same locations 1 and 2 as above as well as the centerline velocity. In this discussion, turbulence settings are set to $Pr_t = Sc_t = 0.9$. The influence of A_{edm} on the velocity is very limited: minimal at the axial measurement locations and slightly more pronounced along the centerline. There is an influence on the size of the upper recirculation zone directly behind the strut. Regarding the lower wall pressure, a different EDM setting does not strongly affect the profile. This can be understood from the fact that the width of the reaction zone along the combustor is not influenced by the combustion model which is shown in the temperature profiles. It is however influenced by the interaction between the shock waves and the turbulent shear layers, and consequently by the turbulence model. The wall pressure trends are similar to some of the results reported in the literature by Potturi and Edwards [55].

The width of the reaction zone predicted by Eilmer with different EDM settings is in good agreement with the experiment.

At the first measurement location, the mean temperature follows the experimental trend well. Peak values in the two shear layers are strongly influenced by the A_{edm} setting. It is difficult to state which setting is more appropriate as not enough experimental data points are available in the shear layer to shed light on the observed peak temperature values. It can be inferred that a value for A_{edm} higher than 1 and below 4 is required. Adopting $A_{edm} = 1$ results in an under-prediction of the peak mean temperature in the lower shear layer at the first measurement location. At the second location the same effect of the EDM setting is observed: higher value coupled with increased peak temperature. In order to match the experimental peak, A_{edm} should be set to ≈ 4. However, a double peak profile is predicted by the CFD which is not experimentally observed. Gonzalez-Juez et al.[57] mentioned in a review paper that a similar observation has been reported in the literature in an LES study with the Eddy Break Up (EBU) model for TCI treatment. The latter model is closely related to the EDM. Nevertheless, the observations are in accordance with the above stated expectations of the EDM: in the vicinity of the strut (a region with higher values of ω) a lower A_{edm} setting is more appropriate while further away (a region with lower values of ω) a higher A_{edm} setting performs better. Overall the standard setting of 4 is a good compromise for the DLR combustor.

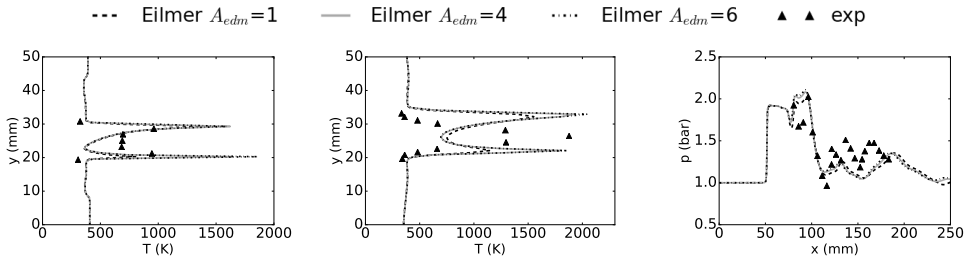

(a) (b) (c)

Figure 16: Effect of the model constant A_{edm} on the temperature at axial locations 1 (a) and 2 (b), and on the wall pressure (c). Results obtained with $Pr_t = Sc_t = 0.9$.

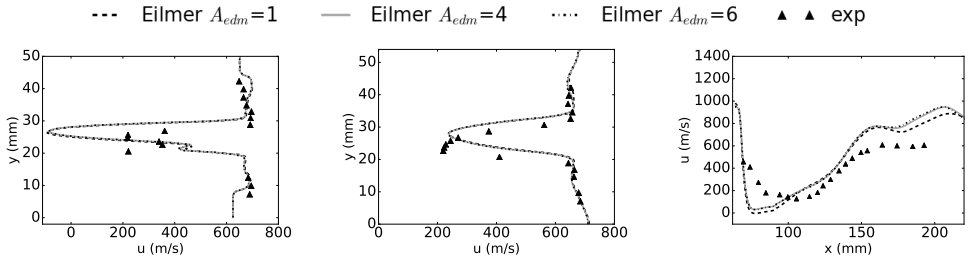

(a) (b) (c)

Figure 17: Effect of the model constant A_{edm} on the velocity at axial locations 1 (a) and 2 (b), and on the centerline velocity (c). Results obtained with $Pr_t = Sc_t = 0.9$.

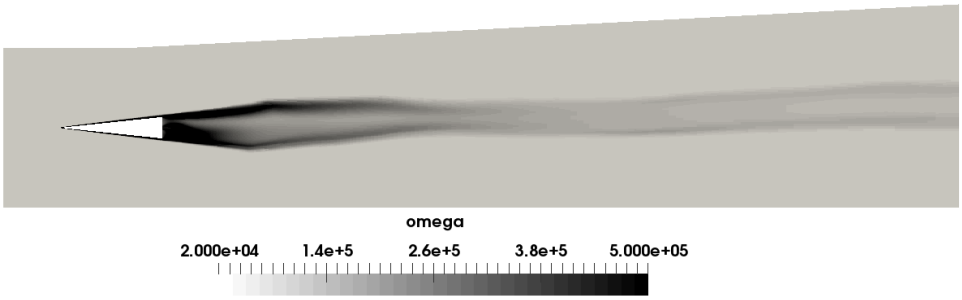

Figure 18: Contour of ω for the DLR combustor experiment of Waidmann et al.[31]

3.3 Case 3: The HyShot II combustor

The HyShot II combustor was designed for a Mach 8 flight test experiment on supersonic combustion[32,33]. Experimental campaigns have been undertaken in the HEG Shock tunnel of the DLR with a 1:1 scale representation using hydrogen fuel. The configuration has been studied with different RANS approaches in the literature[32,33,34]. A detailed description of the ground test experiment is given by Karl[33] and is considered for numerical study in the present work.

3.3.1 Problem Formulation

This simulation is performed in three dimensions, whereas the earlier cases were two dimensional. Only a part of the combustor, shown in Figure 19, is considered for application of the EDM. It consists of half an injector and two symmetry planes. The injector is modeled as a supersonic inflow boundary with conditions: w = 1206.7 m/s , p = 263720 Pa, T = 249 K, I = 5 %, μ_t/μ = 10. The resulting equivalence ratio is 0.29. The upper and lower boundaries (z coordinates) are treated as viscous isothermal walls at a temperature of 300 K. Compressible wall functions of Nichols and Nelson[58] are adopted as to reduce the computational cost of the simulation due to grid requirements . The computational domain is discretized in $\approx$ 2.8M hexahedral cells and an O-grid topology is adopted for the injector. Pecnik et al.[34] obtained satisfactory reacting wall pressure traces with a structured grid consisting of 2.6M cells. Moreover, the injector was modeled as part of the computational domain which extended to include a part of the nozzle. This indicates that the current mesh size of 2.8M cells is a good starting point. In order to ascertain the suitability of the grid for the Eilmer CFD solver, future work should include a mesh independence study. Inviscid fluxes are treated with the AUSMDV and time stepping with a predictor-corrector scheme. Values for turbulent Prantl and Schmidt numbers are set to 0.9 and 0.7 respectively. Sensitivity studies to these parameters have been reported by Karl[33] and Pecnik et al.[34] with the Spalart-Allmaras and the k-ω SST turbulence model respectively. It was observed by both authors that the resulting pressure traces with different combination remain between the experimental uncertainty of the measurements. Therefore, such a sensitivity with the k-ω 2006 model is not considered in the present work. Instead, the standard setting for these parameters is selected. The two-dimensional CFD inflow conditions of Karl et al.[32,33] are prescribed at the inlet of the

three-dimensional domain (same inflow for each lateral cell location) and correspond to averaged conditions: T = 1300 K, p = 130 kPa, u = 1720 m/s and Mach = 2.4. The boundary layer (BL) along the upper wall (cowl side) is assumed to be fully turbulent while a transition from laminar to turbulent flow takes place at the lower wall (injector side) around x = 45 mm. This is accounted for in Eilmer by generating two turbulent zones across the width of the domain, shown in Figure 19. Outside these zones the turbulent quantities (k,ω) are purely transported and do not affect the other governing equations.

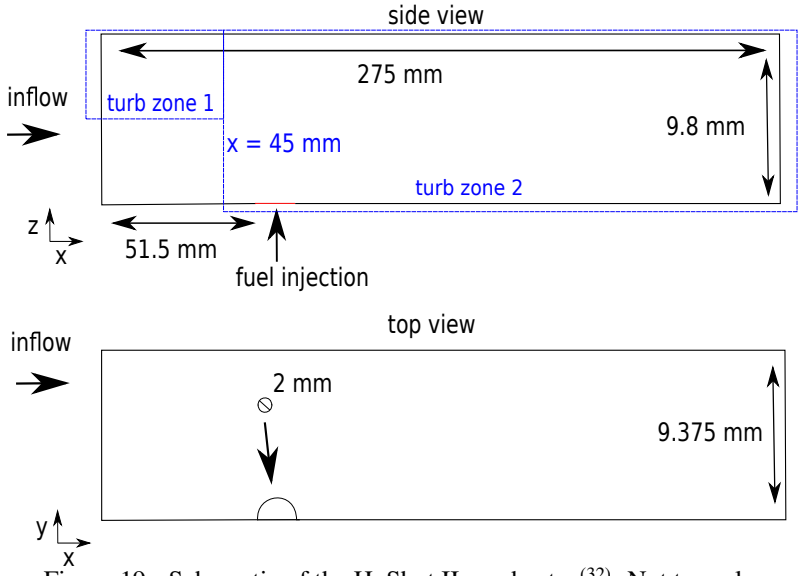

Figure 19: Schematic of the HyShot II combustor[32]. Not to scale.

3.3.2 Results

Reacting simulations of the HyShot II combustor have been performed with the EDM. It was not possible to converge toward a steady-state. It is likely there is an inherent unsteadiness in the flow that has been resolved by the time-accurate explicit time stepping, hence it is an unsteady (URANS) simulation. URANS requires small enough time steps in order to capture variations in mean flow properties due to the largest turbulent fluctuations. Karl et al.[59] reported a study of the unsteady shock train inside the HyShot II combustor. The authors applied URANS with a second order accurate temporal discretization scheme and physical time steps of 1e-7s. The predictor-corrector scheme used in Eilmer is second order accurate[60] and time steps in current HyShot simulations were below 4e-9 s. It can therefore be concluded that URANS is performed in the present work, hence explaining the unsteadiness of the solutions. Note that the non-reacting simulations did converge to a steady state. It can therefore be inferred that the unsteadiness originates due to the injection of fuel (shear driven instability) and / or the combustion process. In order to compare the URANS solutions to the experimental data, time-averaging is applied.

The effect of varying the value of A_{edm} on the wall pressure is investigated in Figures 20

and 21. Increasing the value does result in increased pressure values and an overall vertical shift of the profile. This effect is more pronounced when comparing the curves of A_{edm} = 4 and 6 with respect to the curves of A_{edm} = 2 and 4. On the injector side in Figure 21, an upstream shift of the shock reflection positions is induced by an increased A_{edm} value. The cowl wall pressure trace is in good agreement with the experimental data for any choice of A_{edm}. On the injector side, the pressure traces are within the experimental uncertainty for most of the combustor length. Close to the axial injection location (≈ 52.5 - 120 mm), the EDM is unable to account for the experimental pressure variation. A similar observation is made for the CFD predictions obtained by Karl[33] which is shown in Figure 22 (b). The reference CFD results are predicted by the Tau code with the Spalart-Allmaras turbulence model in conjunction with a no-model chemistry (modified Jachimowski mechanism) approach. The same setting for Pr_t and Sc_t as in the present work were used. Note that Pecnik et al.[34] showed more success in capturing the injector side wall pressure trace with a flamelet TCI model. On the cowl side (Figure 22 (a)), the EDM pressure trace demonstrates a similar trend to the reference CFD. In terms of shock strength, A_{edm} = 6 agrees better with Tau. The pressure profiles in Figures 20 and 21 have been integrated as to obtain the pressure force and averaged pressure. The same has been performed for the experimental values with results shown in Table 3. Given the limited amount of experimental measurements, the latter quantities should be seen as an indication more than an absolute reference point. The Exp_{min} and Exp_{max} are calculated based on the error bars. On the injector side, the pressure force calculated with the different EDM simulations over predict the experimental maximum. This result is probably due to the pressure prediction between ≈ 52.5 - 120 mm and the lack of experimental data in this region. Nevertheless, in terms of averaged pressure, simulations with different A_{edm} settings are within the experimental bounds. On the cowl side, the same observation is made as for the injector side with regard to the averaged pressure values. The pressure force computed for A_{edm} = 2 and 4 are within the experimental bounds while it is overestimated for A_{edm} = 6.

Table 3: Averaged pressure and pressure force predicted by the EDM for the HyShot II combustor.

	Exp_{min}	**Exp_{avg}**	**Exp_{max}**	**A_{edm} = 2**	**A_{edm} = 4**	**A_{edm} = 6**
			Injector wall			
pressure force (kN)	39.4	45.0	50.4	52.5	53.0	54.5
averaged pressure (kPa)	162.5	185.7	207.9	190.1	192.7	198.2
			Cowl wall			
pressure force (kN)	43.3	48.3	53.9	52.7	53.1	54.7
averaged pressure (kPa)	170.1	189.7	211.9	191.5	193.1	198.8

Regarding the use of the EDM for the HyShot II combustor the following conclusions can be drawn. Based on the comparison in Table 3, it could be inferred that the value of A_{edm} should be kept below 6. The wall pressure traces in Figures 21 and 20 do confirm this statement. A higher setting would result in even higher peak values which would not agree with experimental measurements till ≈ 200 mm downstream inside the combustor. Further downstream the strength of the combustion is less intense and the CFD predictions are near the lower part of the experimental uncertainty interval, especially on the cowl side. The observation can be explained with the contour of ω in Figure 23. The turbulent dissipation rate is strong inside the barrel shock induced by fuel injection. This is shown in the different

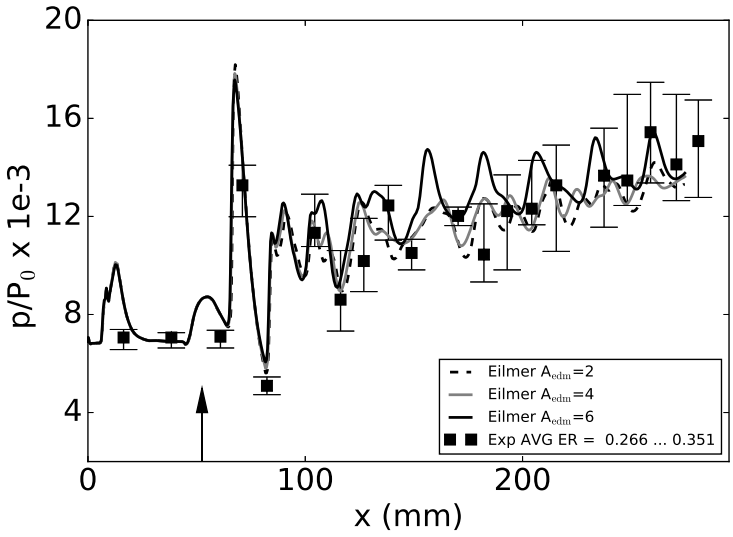

Figure 20: Effect of A_{edm} on the pressure traces along the cowl wall at y = 9.375 mm with P_0 = 17.73 MPa.

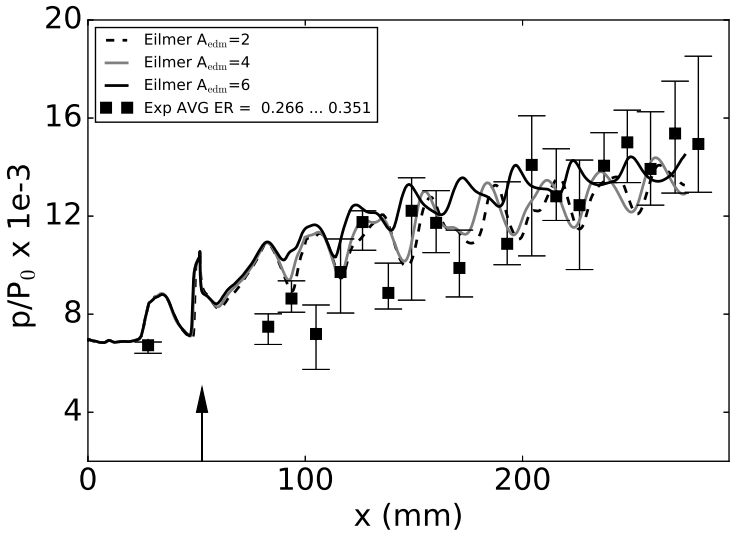

Figure 21: Effect of A_{edm} on the pressure traces along the injector wall at y = 9.375 mm and P_0 = 17.73 MPa.

cross planes. However, moving downstream, the strength reduces considerably (see locations x = 0.15, 0.2 and 0.275 m). In analogy with the Burrows-Kurkov and DLR configurations,

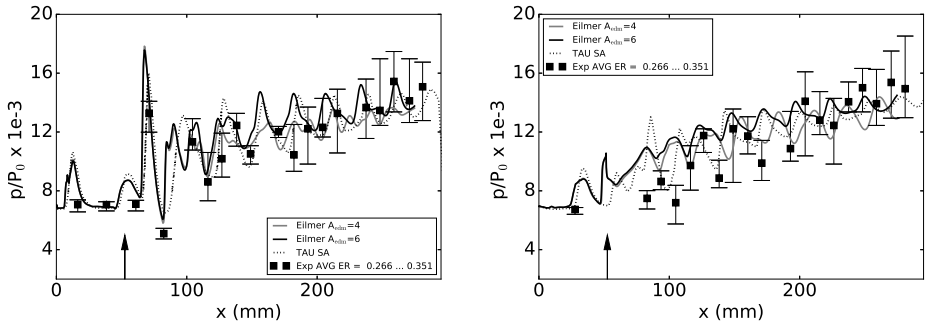

(a) (b)

Figure 22: Pressure along the wall at y = 9.375 mm with EDM and no-model reference CFD: (a) cowl side, (b) injector side. P_0 = 17.73 MPa.

a possibility would be to split the combustor in two zones with a higher A_{edm} value in the more downstream region. Overall, a setting A_{edm} between 4 and 6 is adviced for the HyShot II combustor.

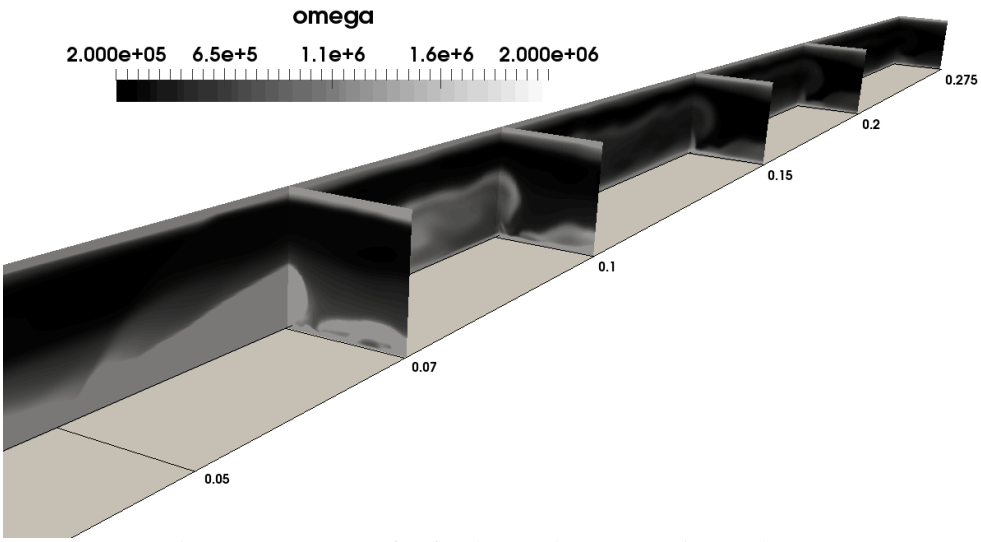

Figure 23: Contour of ω for the HyShot II scramjet combustor.

4.0 DISCUSSION

The experiment of Burrows-Kurkov, the DLR combustor and the HyShot II combustor have been selected in order to investigate the most suitable application of the EDM to supersonic combustion test cases.

In the first test case, the best agreement with several sets of experimental data at the exit of the combustor was achieved with a A_{edm} setting of 6. The value is explained by the configuration with parallel injection of fuel and oxidizer which introduces an ignition delay. In order to capture a similar effect with the EDM, a kinetic limit can be introduced, however the influence is very localized to the near injector region and does not allow for the desired effect. The reaction rate computed with the EDM relies on the value of ω. Its value is high in the shear layer near the injector and decreases downstream the combustor. In other words, in the region where experimentally no combustion should take place, based on the turbulence, the EDM will predict high reaction rates. In the downstream region the opposite is true which explains the need for a high A_{edm} value. An alternative to the kinetic limit has been explored in this work and consists of relying on an estimate of the ignition delay from a one-dimensional chemical kinetics program. A comparison with experimental data demonstrated that the approach resulted in improved predictions and could be considered for the design of similar scramjet configurations. This was termed a zonal EDM approach.

The DLR test case involves fuel injection behind a strut. Application of the kinetic limited resulted in worse agreement with experimental data in the vicinity of the injector. Varying the EDM constant's value did not strongly affect other quantities than the temperature. Just behind the strut, a value between 1 and 4 allows capturing of the experimental temperature profile. Further downstream a value of 4 or higher is more appropriate. These settings are explained by a similar behavior of the turbulence model as in the Burrows-Kurkov test case: high ω values near injector, decreasing downstream. Based on the numerical results of the DLR combustor with the EDM, a suggestion for a modification could be made. Namely, the introduction of a zonal dependency of the A_{edm} value. Close to the point of injection, a lower ($\approx$ 1-4) setting of the A_{edm} constant could be used and further downstream a higher value ($>$ 4). Waidmann et al.[31] discussed the main features inside a configuration such as the DLR combustor. The authors explain the presence of three distinct zones dominated by fundamentally different physics. Firstly there is an induction zone, just behind the strut, where the combustion is dominated by a diffusion process between the injected fuel and vitiated air stream. It is followed by a transitional zone where large scale structures are developing. These structures originate in the shear layers between the air and fuel stream due to the velocity difference and vorticity is produced. They are responsible for the entrainment of the oxidizer inside the reaction zone. In this zone, the combustion is dominated by convection instead of diffusion. Further downstream, a third zone can be discerned where the turbulent eddies break down and the flow becomes more chaotic. Such information can be used for a better application of the EDM and the idea of a zonal EDM could relate to the different flow characteristics. The extent of the three zones would have to be estimated and the A_{edm} setting adapted. It was shown in the experiment of Burrows and Kurkov that even an estimate of the ignition delay is good enough in order to draw design conclusions with the EDM. The same comment can be made for the DLR combustor. Moreover, the zonal approach could as well be applied to the values of Pr_t and Sc_t.

The HyShot II combustor was selected as a third test case. An A_{edm} setting of 4 provided reasonable predictions of wall pressure traces in comparison with experimental data. Similar to the previous test cases, high values of ω are observed near the point of injection with decreasing value downstream of the combustor. As with the previous test cases, a zonal use of the EDM could be an option to improve agreement with experimental observations.

5.0 CONCLUSIONS

In this work the Eddy Dissipation Model (EDM) has been used in conjunction with Wilcox k-ω 2006 turbulence model to the study of three scramjet combustors. A different fuel injection strategy is applied in each of the test cases allowing a broader assessment of the EDM's application. The designs of two of the test cases result in high combustor entrance Mach number (> 2) and static temperature (> 1000 K), typical for high flight Mach numbers while one test case was characterized by cold inflow. The EDM requires the specification of a model constant A_{edm} and the aim of the present work was to understand its most appropriate setting. In the case of parallel fuel injection, a significant ignition delay is present for which the standard application of the EDM, or the EDM with kinetic limit, is unable to account. By relying on an estimate of the ignition delay obtained from a one-dimensional chemical kinetics program, the EDM predictions are in very good agreement with experimental measurements. This indicates that past the point of ignition the combustion appears to be mixing-limited. Without an ignition delay estimate an A_{edm} value of 6 resulted in the best agreement with experimental data while a value of 4 is preferred when an ignition delay is estimated. In the case of fuel injection behind a strut, the EDM with kinetic limit failed to predict one of the reaction zones near the strut and was not considered in further simulations. Regarding the setting of the A_{edm} constant, a value of 4 provided overall reasonable results. In the case of transverse fuel injection, ignition occurs almost as soon as the reactants meet, hence mixing-limited combustion is prevalent. The wall pressure traces obtained with the EDM agreed well with experiments for the majority of the combustor length. Some differences are observed at the injector wall, especially near the point of injection. An A_{edm} constant value of 4 was identified as appropriate in simulating this combustor. In the discussion of the test cases, a zonal use of the EDM was identified as a viable approach to improve the predictive capability of the model and should be explored in future work. Overall, the studies indicate the potential of the EDM to be considered in the design of scramjet combustors with similar configurations.

ACKNOWLEDGEMENTS

The authors would like to express their gratitude to Dr. Peter Jacobs from the University of Queensland for the many discussions and suggestions during the realization of this work. The first author would like to thank Dr. Sebastian Karl at DLR for providing the inflow conditions of the HyShot II combustor. This work was supported by the Royal Society of Edinburgh through the J.M.Lessells scholarship, the University of Strathclyde and the University of Glasgow through the Mac Robertson scholarship. Results were obtained using the EPSRC funded ARCHIE-WeSt High Performance Computer (www.archie-west.ac.uk). EPSRC grant no. EP/K000586/1.

REFERENCES

1. D. Preller and M.K. Smart. Scramjets for reusable launch of small satellites. In *20th AIAA International Space Planes and Hypersonic Systems and Technologies Conference*, page 3586, 2015.
2. SO Forbes-Spyratos, MP Kearney, MK Smart, and IH Jahn. Trajectory design of a rocket-scramjet-rocket multi-stage launch system. In *21st AIAA International Space Planes and Hypersonics Technologies Conference*, page 2107, 2017.

3. Antonio Ferri. Mixing-controlled supersonic combustion. *Annual Review of Fluid Mechanics*, 5(1):301–338, 1973.
4. Antonella Ingenito and Claudio Bruno. Physics and regimes of supersonic combustion. *AIAA Journal*, 48(3):515, 2010.
5. Will O Landsberg, Vincent Wheatley, and Ananthanarayanan Veeraragavan. Characteristics of cascaded fuel injectors within an accelerating scramjet combustor. *AIAA Journal*, pages 3692–3700, 2016.
6. T.F. O'Brien, R.P. Starkey, and M.J. Lewis. Quasi-one-dimensional high-speed engine model with finite-rate chemistry. *Journal of propulsion and power*, 17(6):1366–1374, 2001.
7. Michael Smart. Scramjets. *The Aeronautical Journal*, 111(1124):605–619, 2007.
8. T Vanyai, M Bricalli, S Brieschenk, and RR Boyce. Scramjet performance for ideal combustion processes. *Aerospace Science and Technology*, 75:215–226, 2018.
9. Sean M Torrez, James F Driscoll, Matthias Ihme, and Matthew L Fotia. Reduced-order modeling of turbulent reacting flows with application to ramjets and scramjets. *Journal of propulsion and power*, 27(2):371–382, 2011.
10. RA Baurle. Modeling of high speed reacting flows: established practices and future challenges. *AIAA paper*, 267:2004, 2004.
11. NJ Georgiadis, DA Yoder, MA Vyas, and WA Engblom. Status of turbulence modeling for hypersonic propulsion flowpaths. *Theoretical and Computational Fluid Dynamics*, 28(3):295–318, 2014.
12. BF Magnussen and BH Hjertager. On mathematical modeling of turbulent combustion with special emphasis on soot formation and combustion. In *Symposium (international) on Combustion*, volume 16, pages 719–729. Elsevier, 1977.
13. Jack R Edwards and Jesse A Fulton. Development of a RANS and LES/RANS flow solver for high-speed engine flowpath simulations. In *20th AIAA International Space Planes and Hypersonic Systems and Technologies Conference*, page 3570, 2015.
14. TO Mohieldin, SN Tiwari, and David E Reubush. Numerical investigation of dual-mode scramjet combustor with large upstream interaction. 2004.
15. MSR Chandra Murty and D Chakraborty. Numerical simulation of angular injection of hydrogen fuel in scramjet combustor. *Proceedings of the Institution of Mechanical Engineers, Part G: Journal of Aerospace Engineering*, 226(7):861–872, 2012.
16. M Dharavath, P Manna, and D Chakraborty. Thermochemical exploration of hydrogen combustion in generic scramjet combustor. *Aerospace Science and Technology*, 24(1):264–274, 2013.
17. O.R. Kummitha, K.M. Pandey, and R. Gupta. Cfd analysis of a scramjet combustor with cavity based flame holders. *Acta Astronautica*, 2018.
18. RJ Gollan and PA Jacobs. About the formulation, verification and validation of the hypersonic flow solver Eilmer. *International Journal for Numerical Methods in Fluids*, 73(1):19–57, 2013.
19. DC Wilcox. Formulation of the k-ω turbulence model revisited. *AIAA Journal*, 46(11):2823–2838, 2008.

20. WYK Chan, PA Jacobs, and DJ Mee. Suitability of the k–ω turbulence model for scramjet flowfield simulations. *International Journal for Numerical Methods in Fluids*, 70(4):493–514, 2012.

21. J.J.O.E. Hoste, V. Casseau, M. Fossati, I.J. Taylor, and R.J. Gollan. Numerical modeling and simulation of supersonic flows in propulsion systems by open-source solvers. In *21st AIAA International Space Planes and Hypersonics Technologies Conference*, page 2411, 2017.

22. Jimmy-John O.E. Hoste, M. Fossati, I.J. Taylor, and R.J. Gollan. Modeling scramjet supersonic combustion via eddy dissipation model. In *68th International Astronautical Congress (IAC), Adelaide*, 2017.

23. MN Macrossan. The equilibrium flux method for the calculation of flows with non-equilibrium chemical reactions. *Journal of Computational Physics*, 80(1):204–231, 1989.

24. M.S. Liou. Ten years in the making - AUSM-family. *AIAA Paper*, pages 2001–2521, 2001.

25. PA Jacobs, RJ Gollan, AJ Denman, BT O'Flaherty, DF Potter, PJ Petrie-Repar, and IA Johnston. Eilmer's theory book: basic models for gas dynamics and thermochemistry. Technical report, The University of Queensland, 2012.

26. Sanford Gordon and Bonnie J McBride. *Computer program for calculation of complex chemical equilibrium compositions and applications. I.Analysis*. Citeseer, 1996.

27. T Poinsot and D Veynante. *Theoretical and Numerical Combustion, third edition*. RT Edwards, Inc., 2012.

28. B Sekar and HS Mukunda. A computational study of direct simulation of high speed mixing layers without and with chemical heat release. In *Symposium (International) on Combustion*, volume 23, pages 707–713. Elsevier, 1991.

29. MC Burrows and AP Kurkov. An analytical and experimental study of supersonic combustion of hydrogen in vitiated air stream. *AIAA Journal*, 11(9):1217–1218, 1973.

30. M.C. Burrows and A.P. Kurkov. Analytical and experimental study of supersonic combustion of hydrogen in a vitiated airstream. Technical report, NASA Lewis Research Center, September 1973.

31. W Waidmann, F Alff, U Brummund, M Böhm, W Clauss, and M Oschwald. Experimental investigation of the combustion process in a supersonic combustion ramjet (scramjet). *DGLR Jahrbuch*, pages 629–638, 1994.

32. S. Karl, K. Hannemann, A. Mack, and J. Steelant. CFD analysis of the HyShot II scramjet experiments in the HEG shock tunnel. In *15th AIAA International Space Planes and Hypersonic Systems and Technologies Conference*, page 2548, 2008.

33. Sebastian Karl. *Numerical investigation of a generic scramjet configuration*. PhD thesis, Saechsische Landesbibliothek-Staats-und Universitaetsbibliothek Dresden, 2011.

34. R Pecnik, VE Terrapon, F Ham, G Iaccarino, and H Pitsch. Reynolds-averaged navier-stokes simulations of the hyshot ii scramjet. *AIAA journal*, 50(8):1717–1732, 2012.

35. J Larsson, S Laurence, I Bermejo-Moreno, J Bodart, S Karl, and R Vicquelin. Incipient thermal choking and stable shock-train formation in the heat-release region of a scramjet combustor. part ii: Large eddy simulations. *Combustion and Flame*, 162(4):907–920,

2015.

36. F.R. Menter. Two-equation eddy-viscosity turbulence models for engineering applications. *AIAA Journal*, 32(8):1598–1605, 1994.
37. JS Evans and CJ Schexnayder. Influence of chemical kinetics and unmixedness on burning in supersonic hydrogen flames. *AIAA Journal*, 18(2):188–193, 1980.
38. HB Ebrahimi. CFD validation for scramjet combustor and nozzle flows, part i. *AIAA Paper*, 1840:1993, 1993.
39. B Parent and JP Sislian. Validation of the wilcox k-omega model for flows characteristic to hypersonic airbreathing propulsion. *AIAA Journal*, 42(2):261–270, 2004.
40. WA Engblom, FC Frate, and Nelson CC. Progress in validation of Wind-US for ramjet/scramjet combustion. In *43rd AIAA Aerospace Sciences Meeting and Exhibit*, Reno, Nevada, January 2005.
41. X Xiao, HA Hassan, and RA Baurle. Modeling scramjet flows with variable turbulent Prandtl and Schmidt numbers. *AIAA journal*, 45(6):1415–1423, 2007.
42. P. Keistler. *A variable turbulent Prandtl and Schmidt number model study for scramjet applications*. PhD thesis, 2009.
43. Z Gao, C Jiang, S Pan, and CH Lee. Combustion heat-release effects on supersonic compressible turbulent boundary layers. *AIAA Journal*, 53(7):1949–1968, 2015.
44. JR Edwards, JA Boles, and RA Baurle. Large-eddy/Reynolds-averaged Navier–Stokes simulation of a supersonic reacting wall jet. *Combustion and Flame*, 159(3):1127–1138, 2012.
45. Ji-Ho Kim, Youngbin Yoon, In-Seuck Jeung, Hwanil Huh, and Jeong-Yeol Choi. Numerical study of mixing enhancement by shock waves in model scramiet engine. *AIAA Journal*, 41(6):1074–1080, 2003.
46. V Bhagwandin, W Engblom, and N Georgiadis. Numerical simulation of a hydrogen-fueled dual-mode scramjet engine using Wind-US. In *45th AIAA/ASME/SAE/ASEE Joint Propulsion Conference & Exhibit*, page 5382, 2009.
47. D.A. Bittker and V.J. Scullin. General chemical kinetics computer program for static and flow reactions, with application to combustion and shock-tube kinetics. 1972.
48. RM Kirchhartz, DJ Mee, RJ Stalker, PA Jacobs, and MK Smart. Supersonic boundary-layer combustion: effects of upstream entropy and shear-layer thickness. *Journal of Propulsion and Power*, 26(1):57–66, 2010.
49. M Oevermann. Numerical investigation of turbulent hydrogen combustion in a scramjet using flamelet modeling. *Aerospace science and technology*, 4(7):463–480, 2000.
50. A Mura and JF Izard. Numerical simulation of supersonic nonpremixed turbulent combustion in a scramjet combustor model. *Journal of Propulsion and Power*, 26(4):858–868, 2010.
51. Z Gao, J Wang, C Jiang, and C Lee. Application and theoretical analysis of the flamelet model for supersonic turbulent combustion flows in the scramjet engine. *Combustion Theory and Modelling*, 18(6):652–691, 2014.
52. L Hou, D Niu, and Z Ren. Partially premixed flamelet modeling in a hydrogen-fueled supersonic combustor. *International Journal of Hydrogen Energy*, 39(17):9497–9504,

2014.

53. Obula Reddy Kummitha. Numerical analysis of hydrogen fuel scramjet combustor with turbulence development inserts and with different turbulence models. *International Journal of Hydrogen Energy*, 42(9):6360–6368, 2017.
54. F Génin and S Menon. Simulation of turbulent mixing behind a strut injector in supersonic flow. *AIAA Journal*, 48(3):526, 2010.
55. AS Potturi and JR Edwards. Hybrid Large-Eddy/Reynolds-averaged Navier–Stokes simulations of flow through a model scramjet. *AIAA Journal*, 2014.
56. C Fureby, E Fedina, and J Tegnér. A computational study of supersonic combustion behind a wedge-shaped flameholder. *Shock waves*, 24(1):41–50, 2014.
57. ED Gonzalez-Juez, AR Kerstein, R Ranjan, and S Menon. Advances and challenges in modeling high-speed turbulent combustion in propulsion systems. *Progress in Energy and Combustion Science*, 60:26–67, 2017.
58. Robert H Nichols and CC Nelson. Wall function boundary conditions including heat transfer and compressibility. *AIAA journal*, 42(6):1107–1114, 2004.
59. S Karl, S Laurence, JM Schramm, and K Hannemann. CFD Analysis of Unsteady Combustion Phenomena in the HyShot-II Scramjet Configuration. In *18th AIAA/3AF International Space Planes and Hypersonic Systems and Technologies Conference*, page 5912, 2012.
60. Timothy J Barth and Herman Deconinck. *High-order methods for computational physics*, volume 9. Springer Science & Business Media, 2013.

Dear Editor-in-Chief,

It is with pleasure that we present to you a manuscript entitled “Characterization of the Eddy Dissipation Model for the Design of Hydrogen-fueled Scramjets” for consideration for publication in The Aeronautical Journal.

The manuscript discusses the application of the Eddy Dissipation Model (EDM) to describe the turbulent supersonic combustion process inside scramjet propulsion systems by means of CFD approaches.

The EDM needs the specification of modeling constants for which no consistent guidelines are available in the open literature. This work relates the setting of the modeling constants to the flow physics occuring inside typical scramjet configurations. Three widely adopted CFD validation test cases are selected for this task for which experimental data is available. The model is cost-effective, yet capable of providing reasonable predictions of the flow field inside the selected scramjet test cases.

It is our believe that the proposed manuscript combines several topics relevant to The Aeronautical Journal. The application of an existing combustion model to conditions outside it’s original development purpose is discussed. A detailed description of the model including possibilities to extend it are given with a practical application in mind, namely its use for preliminary design of scramjets. This work has not been published or submitted for publication anywhere else.

We are very grateful for your consideration of our manuscript and we look forward to your response as well as the one of the reviewers.

Best regards,

Jimmy-John O.E. Hoste, Marco Fossati, Ian J. Taylor and Rowan J. Gollan

Corresponding author
Jimmy-John O.E. Hoste
3/6, 161 High Street
G11XJ, Glasgow
United Kingdom
jimmyjohn.hoste@gmail.com